Detecting and exploiting chaotic transport in mechanical systems

Shane D. Ross and Phanindra Tallapragada

Abstract Several geometric and probabilistic methods for studying chaotic phase space transport have been developed and fruitfully applied to diverse areas from orbital mechanics to biomechanics to fluid mechanics and beyond. Increasingly, systems of interest are determined not by analytically defined model systems, but by data from experiments or large-scale simulations. We will discuss those features of phase space transport in finite-time systems which seem to be robust, considering invariant manifolds and invariant manifold-like objects, and their connection with concepts such as symbolic dynamics, chaos, almost-invariant sets, and coherent sets. We end with an application to efficient movement of weakly propelled vehicles in fluid flows.

1 Introduction

Several geometric and probabilistic methods for studying chaotic phase space transport have been developed and fruitfully applied to diverse areas from orbital mechanics, chemistry, biomechanics to fluid mechanics and beyond [1–31]. There is much interest in understanding how chaos arises in dynamical systems, how to detect it, how to exploit it when it is present, and how to design for (or against) it [32]. Increasingly, systems of interest are determined not by analytically defined model systems, but by data from experiments or large-scale simulations from many areas of the physical sciences, including atomic physics [4], geophysical fluid dynamics [33–37], musculoskeletal biomechanics [38–45], and space mission design [1, 46–51]. We will discuss those features of chaotic phase space transport in finite-

Shane D. Ross
Engineering Science and Mechanics, Virginia Tech, Blacksburg, VA, USA e-mail: sdross@vt.edu

Phanindra Tallapragada
Mechanical Engineering and Engineering Science, Univ. of North Carolina at Charlotte, NC, USA
e-mail: phanindra@uncc.edu

time, non-autonomous systems which seem to be robust, considering invariant manifolds and invariant manifold-like objects, and their connection with concepts such as symbolic dynamics [1], braids [52–55], chaos, almost-invariant sets [18, 56], and coherent sets [22].

These methods fall into two main categories, the geometric and the probabilistic. Under the umbrella of geometric methods are the techniques of invariant manifolds (of fixed points or larger invariant sets) [1–4, 57], lobe dynamics [18, 37, 58, 59], finite-time Lyapunov exponents (FTLE) and Lagrangian coherent structures (LCS) [35, 60–65]. The method of FTLE-LCS has proven to be particularly useful in studying transport in time-dependent systems and has found a variety of applications [25–30]. The probabilistic approach studies the transport of densities and measures and the so-called almost invariant sets (AISs) and coherent sets. These methods too have been successfully applied in the study of various geophysical flow problems [22] and mixing in microchannels [31].

The development of the above two methods to non-autonomous settings has occurred almost simultaneously in the last decade. The geometric methods, particularly FTLE-LCS, study stretching and contraction around reference trajectories and identify transport barriers. The FTLE-LCS method is therefore a local method; it provides local transport information from which one attempts to infer the global transport properties of the system. The probabilistic method, on the other hand, ignores the local transport structures, but using the transfer operator divides the phase space into maximally invariant sets.

One engineering application we consider is the determination of optimal routes for weakly propelled immersed in complex environmental fluid flows, by developing control schemes which explicitly incorporate the geometry of the dynamical structures which organize the flow. We consider the methods we describe as a stepping stone to a formal linking between the theory of chaotic transport and optimal control.

2 Computing Chaotic Transport

The theory of transport in phase space is a unified mathematical description of dynamical processes that can be applied to a wide range of physical phenomena across many scales. A geometric picture describing transport is emerging for time-chaotic (aperiodic) flow fields [1–3, 18, 28, 41, 47–50, 66–75]. The key is to partition the phase space into subsets and then to identify how phase points travel within and between the subsets [18]. In time-periodic systems, the stable and unstable manifolds of normally hyperbolic invariant manifolds (NHIMs) [1, 2, 76]—e.g., fixed points, periodic orbits, or other bound sets or orbits—provide the co-dimension one separatrices.

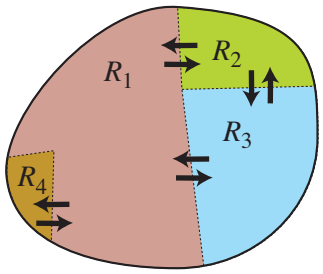

Fig. 1 The manifold M is partitioned into the regions $R_i, i = 1,\ldots,N_R$. If points are distributed uniformly over M at $t = 0$, we want to compute the movement of points between these regions for all times $t > 0$.

2.1 Transport Between Regions in Phase Space

To make the description of phase space transport more precise, consider the following. Suppose we have a volume- and orientation-preserving map $f : M \to M$ (e.g., a time-T (stroboscopic) map ϕ_t^{t+T} or a Poincaré map resulting from a continuous time dynamical system) on some compact set $M \subset \mathbb{R}^n$ with volume-measure μ and we seek a suitable (i.e. depending on the application in mind) *partition* of M into compact *regions of interest* R_i, $i = 1,\ldots,N_R$, as shown schematically in Fig. 1, such that

$$M = \bigcup_{i=1}^{N_R} R_i \quad \text{and} \quad \mu(R_i \bigcap R_j) = 0 \text{ for } i \neq j. \tag{1}$$

Furthermore, we are interested in the following questions concerning the transport between the regions R_i (see [77]): In order to keep track of the initial condition of a point as it moves throughout the regions, we say that initially (i.e., at $t = 0$) region R_i is uniformly covered with species S_i. Thus, the species type of a point indicates the region in which it was located initially. Then we can generally state the transport problem as follows.

Describe the distribution of species S_i, $i = 1,\ldots,N_R$, throughout the regions R_j, $j = 1,\ldots,N_R$, for any time $t = n > 0$.

The quantity we want to compute is $T_{i,j}(n) \equiv$ *the total amount of species S_i contained in region R_j immediately after the n-th iterate.*

The *flux* $\alpha_{i,j}(n)$ of species S_i into region R_j on the n-th iterate is the change in the amount of species S_i in R_j on iteration n; namely, $\alpha_{i,j}(n) = T_{i,j}(n) - T_{i,j}(n-1)$. Since f is assumed volume-preserving, the flux is equal to the amount of species S_i entering region R_j at iteration n minus the amount of species S_i leaving R_j at iteration n.

Our goal is to determine $T_{i,j}(n), i, j = 1,\ldots,N_R$ for all n. Note, that $T_{i,i}(0) = \mu(R_i)$, and $T_{i,j}(0) = 0$ for $i \neq j$. In the following we briefly describe the theoretical background behind the two computational approaches to the transport problem.

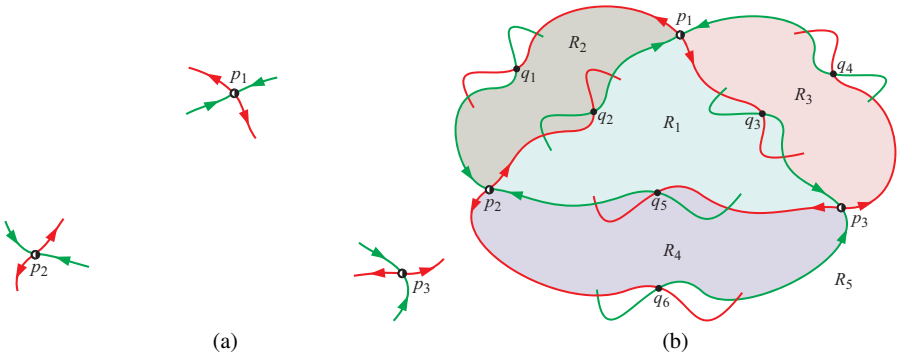

Fig. 2 (a) Pieces of the local unstable and stable manifolds, $W^u(p_i)$ (red) and $W^s(p_i)$ (green) of saddle fixed points $\{p_i\}$. (b) When the manifolds $W^u(p_i)$ and $W^s(p_i)$ are followed out on a global scale, they often intersect in primary intersection points $\{q_i\}$. These intersections allow one to define boundaries betweens regions $\{R_i\}$.

2.2 Lobe Dynamics

Lobe dynamics theory has been developed for the case $n = 2$ [58] and states that the two-dimensional phase space M of the map f can be divided as outlined above (see eq. (1)). We define a region to be a connected subset of M with boundaries consisting of parts of the boundary of M (which may be at infinity) and/or segments of stable and unstable invariant manifolds of saddle-type hyperbolic fixed points, $p_i, i = 1,...,N$, as shown schematically in Fig. 2(a). When the manifolds $W^u(p_i)$ and $W^s(p_i)$ are followed out on a global scale, they often intersect in primary intersection points $\{q_i\}$. These intersections allow one to define boundaries betweens regions $\{R_i\}$, as illustrated in Fig. 2(b). Moreover, the transport between regions of phase space can be completely described by the dynamical evolution of small subregions of phase space, "lobes" enclosed by segments of the stable and unstable manifolds as defined below.

Boundaries, Regions, Pips, Lobes, and Turnstiles Defined. In order to define a *boundary* between regions, we must first define a *primary intersection point*, or *pip*. Consider just two saddle points, p_i and p_j. Suppose $W^u(p_i)$ and $W^s(p_j)$ intersect transversally at least once, i.e., $W^u(p_i) \bigcap W^s(p_j) \neq \emptyset$. Then by the definition of stable and unstable manifolds, they must intersect an infinite number of times. Consider just two of these intersection points, q and $\bar{q}$, as in Fig. 3. An intersection point r is a pip if $U[p_i, r]$ intersects $S[r, p_j]$ only at the point r, where $U[p_i, r]$ and $S[r, p_j]$ are segments of the unstable and stable manifolds, $W^u(p_i)$ and $W^s(p_j)$, respectively. In Fig. 3, q is a pip, but $\bar{q}$ is not a pip. The union of segments of the unstable and stable manifolds, which terminate in a pip, naturally form *boundaries* between *regions*. Considering Fig. 3(b), define $B \equiv U[p_i, q] \bigcup S[p_j, q]$ as the boundary between "two sides", the regions R_1 and R_2. Note that we could have $p_i = p_j$.

Let $q_0, q_1 \in W^u(p_i) \bigcap W^s(p_j)$ be two adjacent pips, as in Fig. 4(a), i.e., there are no other pips on $U[q_0,q_1]$ and $S[q_0,q_1]$, the segments of $W^u(p_i)$ and $W^s(p_j)$ connecting q_0 and q_1. We refer to the region interior (int) to $U[q_0,q_1] \bigcup S[q_0,q_1]$ as a *lobe*. Now consider again a pip q, as in Fig. 4(b). Since q is a pip, $f^{-1}(q)$ is also a pip; both are part of the heteroclinic orbit passing through q, $h_q = \{\ldots, f^{-2}(q), f^{-1}(q), q, f^1(q), f^2(q), \ldots\}$ asymptotically going from p_i to p_j, i.e., $f^{-n}(q) \to p_i$ and $f^n(q) \to p_j$ as $n \to \infty$. As f is orientation-preserving, there is at least one pip on $U[f^{-1}(q), q]$ where the $W^u(p_i), W^s(p_j)$ intersection is topologically transverse. Let us assume there is only one such pip, called q_1, as illustrated in Fig. 4(b); it belongs to a distinct heteroclinic orbit $h_{q_1} \neq h_q$ connecting p_i and p_j. Then $S[f^{-1}(q), q] \bigcup U[f^{-1}(q), q]$, highlighted in Fig. 4(c), forms the boundary of precisely two lobes; one in R_1,

$$L_{1,2}(1) \equiv \text{int}(U[f^{-1}(q), q_1] \bigcup S[f^{-1}(q), q_1]) \tag{2}$$

and the other in R_2,

$$L_{2,1}(1) \equiv \text{int}(U[q_1, q] \bigcup S[q_1, q]). \tag{3}$$

Under one iteration of f, the only points that can move from R_1 into R_2 by crossing B are those in $L_{1,2}(1)$. The amount of phase space transported is $\mu(L_{1,2}(1))$. Similarly, under one iteration of f the only points that can move from R_2 into R_1 by crossing B are those in $L_{2,1}(1)$, where $\mu(L_{2,1}(1) = \mu(L_{1,2}(1)$; see Fig. 4(d). In some cases, $\mu(L_{1,2}(1)$ can be computed from sums of action differences between the heteroclinic orbits h_q and h_{q_1} [78].

The two lobes $L_{1,2}(1)$ and $L_{2,1}(1)$ are called a *turnstile* [79] and individually they are turnstile lobes. The essence of lobe dynamics can be stated as follows: the dynamics associated with crossing B is reduced to the dynamics of the turnstile lobes associated with B.

These results generalize to the boundary between any two sets R_i and R_j. We have chosen our notation such that $L_{i,j}(m),\ m \geq 2$ denotes the lobe that leaves R_i and enters R_j on the m-th iterate, so that $L_{i,j}(m) = f^{1-m}(L_{i,j}(1))$. It is important to note that $L_{i,j}(m),\ m \geq 2$, need not be contained entirely in R_i, and $f^n(L_{i,j}(1)),\ n \geq 2$,

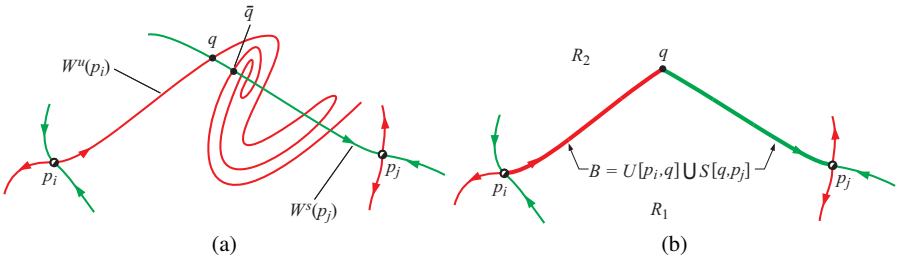

Fig. 3 (a) q is a primary intersection point (pip), while $\bar{q}$ is not. (b) Suppose $q \in W^u(p_i) \bigcap W^s(p_j)$ is a pip. We define $B \equiv U[p_i,q] \bigcup S[q,p_j]$ as a boundary between "two sides," R_1 and R_2.

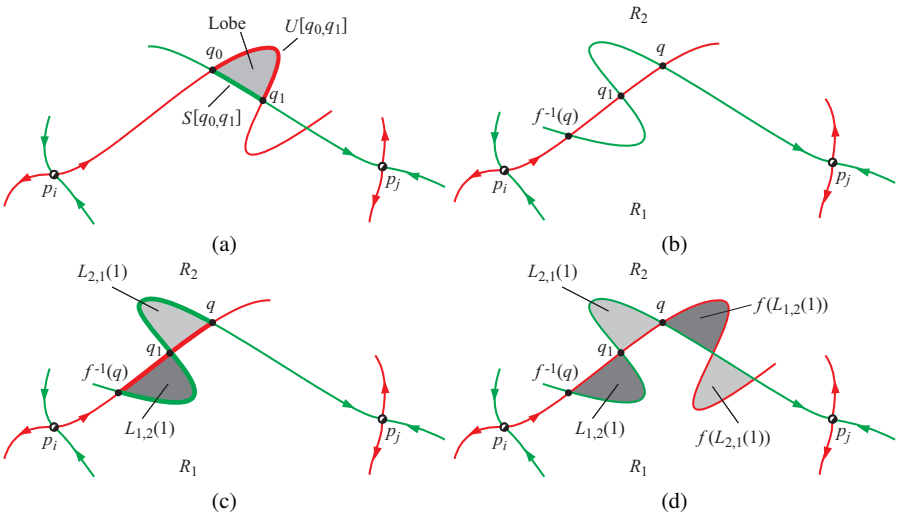

Fig. 4 (a) The region interior to $U[q_0,q_1]\bigcup S[q_0,q_1]$ is a lobe. (b) If q is a pip, so is $f^{-1}(q)$. Also, since f is orientation-preserving there is at least one pip, e.g., q_1, in $U[f^{-1}(q),q]$ where the $W^u(p_i),W^s(p_j)$ intersection is topologically transverse. (c) $U[f^{-1}(q),q]\bigcup S[f^{-1}(q),q]$ forms the boundary of precisely two lobes; one in R_1, labeled $L_{1,2}(1)$, and the other in R_2, labeled, $L_{2,1}(1)$. (d) Under one iteration of f, only points in $L_{1,2}(1)$ can move from R_1 into R_2 by crossing B; and similarly for points in $L_{2,1}(1)$. The two lobes $L_{1,2}(1)$ and $L_{2,1}(1)$ are called a turnstile.

need not be contained entirely in R_j, i.e., the lobes can leave and re-enter regions with strong implications for the dynamics.

We can consider the lobes as prototypes of 'mobile' subregions, 'atoms' of phase space transport, whose images and pre-images under f will visit several regions. As an alternative notation, we can label these subregions based on their itineraries—that is, their past, present, and future whereabouts with respect to the regions $\{R_i\}$. For example, we can label $L_{1,2}(1)$ as $([R_1],R_2)$, where the bracketed region is the current region, and under one iterations of f, the pre-image will be entirely contained in R_2; thus, $f([R_1],R_2) = (R_1,[R_2])$. As in Fig. 5, itinerary labels of subregions can be naturally concatenated according to the labels of their corresponding intersected subregions. With this notation, we can label subregions with complicated itineraries, e.g., $(R_2,R_3,[R_2],R_1,R_5)$, where longer itineraries will belong to smaller regions of phase space. In a later section, we will use these subregion itinerary labels to go between distant regions of the phase space using small controls, e.g., going from region R_4 to region R_1 in the schematic illustration of Fig. 6.

Multilobe, Self-Intersecting Turnstiles. Before going further, some comments regarding technical points are in order [58]. Above we assumed that there was only one pip between q and $f^{-1}(q)$, but this is not the case in all applications. Suppose that there are k pips, $k \geq 1$, along $U[f^{-1}(q),q]$ besides q and $f^{-1}(q)$. This gives rise to $k+1$ lobes; m in R_2 and $(k+1)-m$ in R_1. Suppose

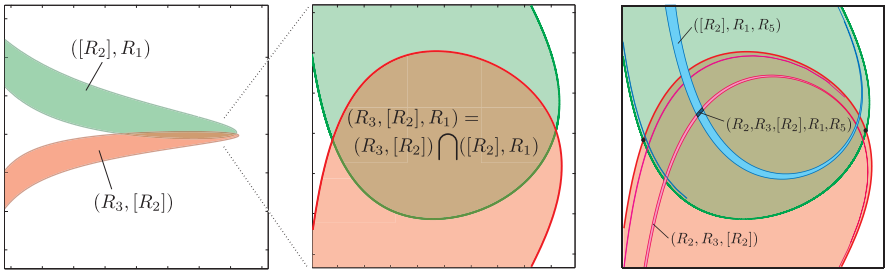

Fig. 5 Consider an example with several regions $\{R_1,R_2,R_3,R_4,R_5\}$, where we seek to label lobe intersections accordingly. (a) Consider two intersecting lobes $([R_2],R_1)$ and $(R_3,[R_2],R_1)$. (b) Zooming-in, denote the intersection $(R_3,[R_2])\bigcap([R_2],R_1)$ by $(R_3,[R_2],R_1)$. (c) Longer itineraries correspond to smaller pieces of phase space.

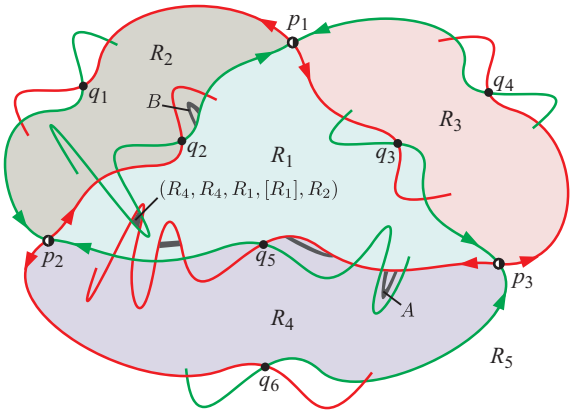

Fig. 6 The same regions as given in Fig. 2(b) are redrawn, this time extending some of the manifolds further to highlight the intersection of manifolds which bounds the subregion with itinerary $(R_4,R_4,R_1,[R_1],R_2)$. The image of this subregion under the map is B, i.e., $B = f(R_4,R_4,R_1,[R_1],R_2) = (R_4,R_4,R_1,R_1,[R_2])$, while $A = f^{-3}(R_4,R_4,R_1,[R_1],R_2) = ([R_4],R_4,R_1,R_1,R_2)$.

$$L_0,L_1,\cdots,L_{k-m} \subset R_1,$$
$$L_{k-m+1},L_{k-m+2},\cdots,L_k \subset R_2.$$

Then we define

$$L_{1,2}(1) \equiv L_0 \bigcup L_1 \bigcup \cdots \bigcup L_{k-m},$$
$$L_{2,1}(1) \equiv L_{k-m+1} \bigcup L_{k-m+2} \bigcup \cdots \bigcup L_k,$$

and all the previous results hold.

An example of a multilobe turnstile comes from the study of orbits around rotating distended asteroids. Using the planar restricted full two-body problem as a model (details provided in [71]), we can consider the trajectories of particles at a constant Hamiltonian energy, viewed on a 2D Poincaré surface-of-section. Particles can be ejected from the system (out to infinity) or captured into the system (from infinity). The phase space structure governing these phenomena is a homoclinic tan-

gle associated with stable and unstable manifolds of a fixed point at infinity. Using (r, p_r) as coordinates along the surface-of-section, where r is the distance from the center of the asteroid and p_r is its conjugate momentum, this point is at $p = (\infty, 0)$. As shown in Fig. 7, the resulting homoclinic tangle has is a multilobe turnstile with $k = 3$ and $m = 2$.

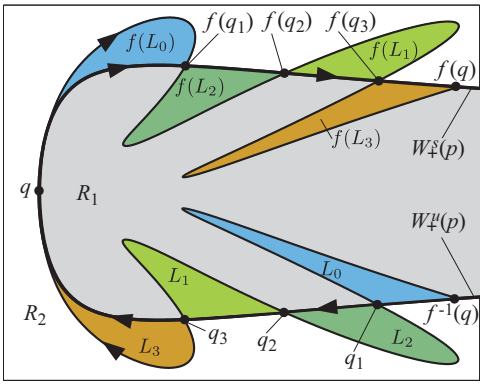

Fig. 7 An example of a multilobe turnstile with $k = 3$, $m = 2$. The system is the motion of a particle (e.g., ejecta) in the field of a rotating asteroid and is a Hamiltonian system. The coordinates shown here are (r, p_r), where r is the distance from the center of the asteroid and p_r is its conjugate momentum.

Furthermore, we previously assumed that $L_{1,2}(1)$ and $L_{2,1}(1)$ lie entirely in R_1 and R_2, respectively. But $L_{1,2}(1)$ may intersect $L_{2,1}(1)$, as shown schematically in Fig. 11(a) for the case of a homoclinic tangle. We want $U[f^{-1}(q), q]$ and $S[f^{-1}(q), q]$ to intersect only in pips, so we must redefine our lobes, as shown in Fig. 11(b). Let

$$I = \text{int}\left(L_{1,2}(1) \bigcap L_{2,1}(1)\right).$$

The lobes defining the turnstile are redefined as

$$\begin{aligned} \tilde{L}_{1,2}(1) &\equiv L_{1,2}(1) - I, \\ \tilde{L}_{2,1}(1) &\equiv L_{2,1}(1) - I, \end{aligned} \tag{4}$$

and all our previous results hold. We note that multilobe, self-intersecting turnstiles [18] do indeed appear in physical systems, and may be a geometric phase space 'constraint' which has a significant impact on the dynamics.

Expressions for the Transport of Species. Complicated transport properties can result from lobe dynamics (cf. [1, 58, 59, 78, 80]). Using the lobe dynamics framework, the transport of species between the regions—$T_{i,j}(n)$—can be computed via the following formulas.

Let $L^k_{i,j}(m) \equiv L_{i,j}(m) \bigcap R_k$ denote the portion of lobe $L_{i,j}(m)$ that is in the region R_k. Then

$$T_{i,j}(n) - T_{i,j}(n-1) = \sum_{k=1}^{2} [\mu(L^i_{k,j}(n)) - \mu(L^i_{j,k}(n))] \tag{5}$$

where

$$\mu(L^i_{k,j}(n)) = \sum_{s=1}^{2}\sum_{m=0}^{n-1} \mu\left(L_{k,j}(1)\bigcap f^m(L_{i,s}(1))\right) - \sum_{s=1}^{2}\sum_{m=1}^{n-1} \mu\left(L_{k,j}(1)\bigcap f^m(L_{s,i}(1))\right). \quad (6)$$

Thus, the dynamics associated with crossing a boundary B is reduced completely to a study of the dynamics of the turnstile lobes associated with B. The amount of computation necessary to obtain all the $T_{i,j}(n)$ can be reduced due to conservation of area and species, as well as symmetries of the map f. In some cases, one can obtain A typical species transport calculation result is given in Fig. 9 where only two regions are considered. Notice that after only a few iterates of the map, a high degree of filamentation is seen.

2.3 Finite-Time Analogs of Invariant Manifolds

The method described above works for systems described by autonomous or time-periodic flow fields. However, time-chaotic flow fields do not, in general, have fixed points or periodic orbits. In this case, co-dimension one surfaces of high hyperbolicity play a role analogous to the stable and unstable manifolds of NHIMs, delineating the boundaries between dynamically distinct regions and identifying lanes

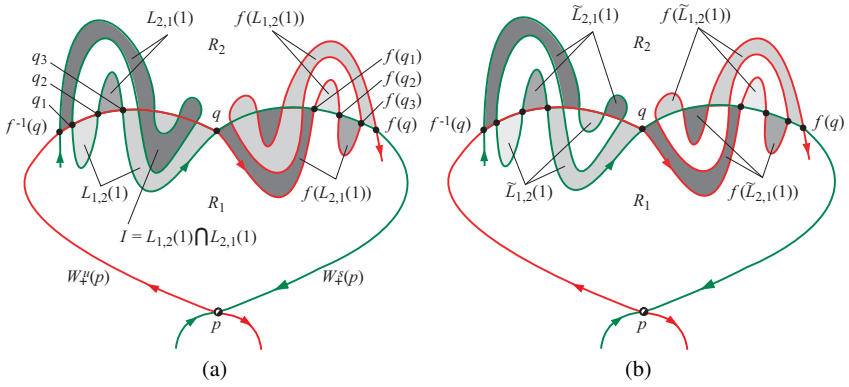

Fig. 8 A multilobe, self-intersecting turnstile. (a) The stable and unstable manifolds of the unstable fixed point p intersect in such a way that there are three pips between q and $f^{-1}(q)$, but our naively defined turnstile "lobes" have a non-empty intersection $I = \text{int}\,(L_{1,2}(1)\bigcap L_{2,1}(1)) \neq \emptyset$. (b) When we redefine the turnstile lobes such that $\tilde{L}_{1,2}(1) \equiv L_{1,2}(1) - I$ and $\tilde{L}_{2,1}(1) \equiv L_{2,1}(1) - I$, the result is a *multilobe, self-intersecting turnstile* consisting of a sequence of six regions; three defining $\tilde{L}_{1,2}(1)$ and three others defining $\tilde{L}_{2,1}(1)$.

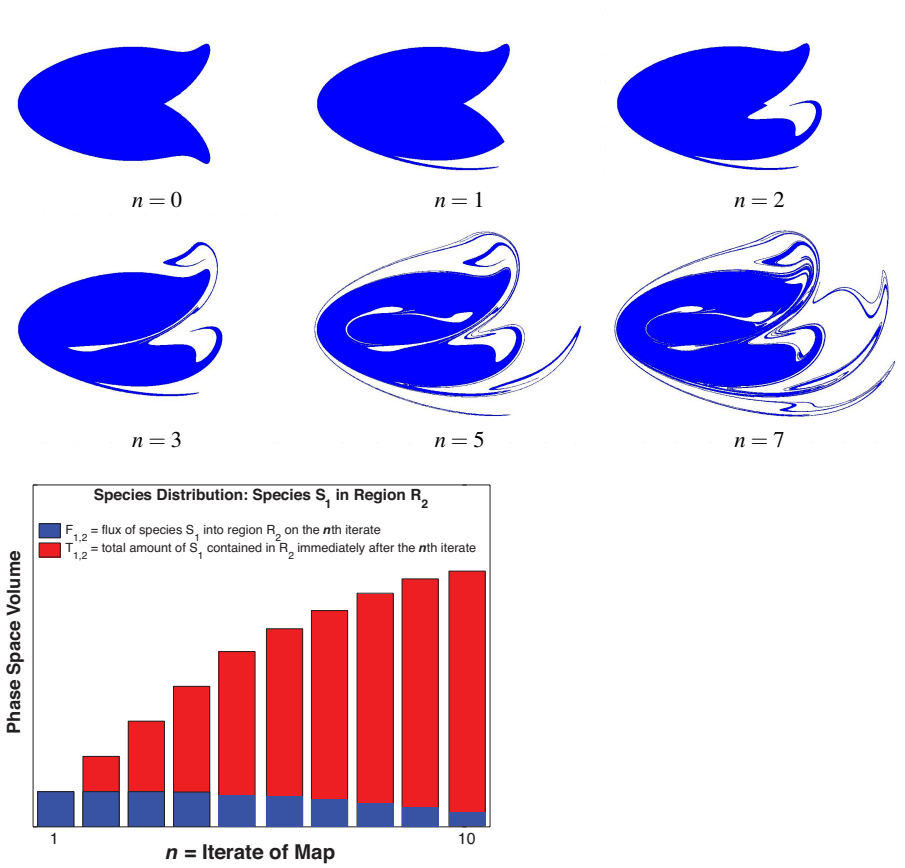

Fig. 9 (upper panels) The two regions at time $n = 0$ define the two species (upper left); S_1 is dark, S_2 is white. Several iterates of S_1 are shown, namely $n = 1, 2, 3, 5, 7$. (lower panel) The flux and total transport of species S_1 into region R_2 are shown as a function of iterate. The (vertical) phase space scale is relative. The example shown here comes from celestial mechanics, specifically the planar circular restricted three-body problem. The 2D state space here is from a Poincaré surface-of-section restricted to a constant energy surface.

of transport. Computations of these surfaces have proven valuable for the analysis of geophysical transport (see Fig. 10). These finite-time hyperbolic manifolds, or Lagrangian coherent structures (LCS) [60, 81], can be obtained from ridges in the time-varying finite-time Lyapunov exponent (FTLE) field [28, 44, 81, 82].

FTLE Definition. For a flow field defined by data sets or a set of ordinary differential equations on a possibly non-Euclidean (i.e., curved) manifold, we define the flow map as $\phi_{t_0}^t : x(t_0) \mapsto x(t)$, which maps phase space points (or particles) from their initial location at time t_0 to their location at time t. We may be interested in FTLE and LCS on curved manifolds, e.g., where geophysical flows live,

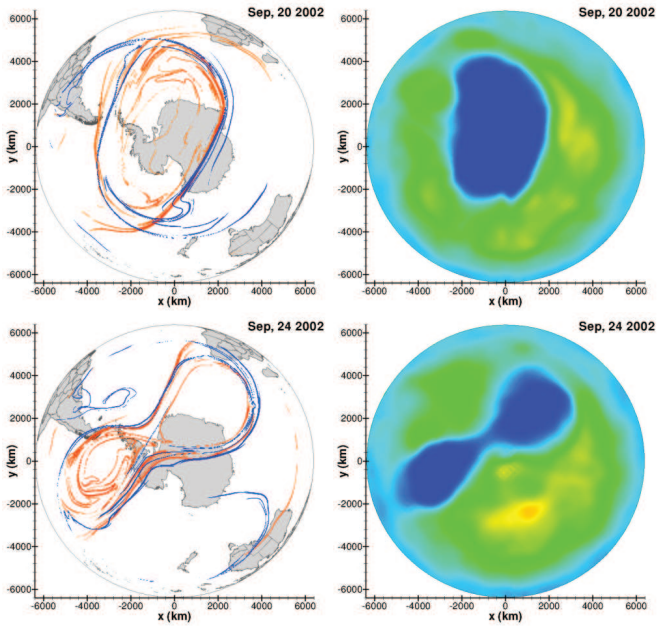

Fig. 10 (Left) Atmospheric LCS for days surrounding the Antarctic polar vortex splitting event of September 2002 (based on NCEP/NCAR reanalysis data using $T = \pm 8$ days); attracting (repelling) curves, analogous to unstable (stable) manifolds of saddle points, are shown in blue (red). Before and after the splitting event in late September, we see an isolated blob of air, bounded by LCS curves, slowly rotating over Antarctica. The vortex pinches off, sending the northwestern part of the ozone hole off into the midlatitudes while the southwestern portion goes back to its regular position over Antarctica. Note the formation of lobes at the edges where chaotic stirring occurs across the LCS. (Right) The corresponding daily ozone concentration (based on NASA TOMS satellite data). The time-varying LCS structures that bound the ozone hole fragments provide a framework for understanding the atmospheric transport. The system can be said to have undergone a 'Duffing bifurcation' given its gross similarity to a Duffing oscillator passing through a critical parameter value.

due to sphericity of the Earth or boundary topography, or to handle curved phase spaces which naturally arise in mechanics, such as $T\mathrm{SO}(3)$ or $T\mathrm{SE}(3)$. We define the FTLE $\sigma(x,t_0,t)$ as the norm of the differential of the flow map $\phi_{t_0}^t$ at the initial point x, i.e.,

$$\sigma(x,t_0,t) = \frac{1}{|t-t_0|}\log\left\|\mathrm{D}\phi_{t_0}^t\right\| \equiv \frac{1}{|t-t_0|}\log\left(\max_{\mathbf{y}\neq\mathbf{0}}\frac{\left\|\mathrm{D}\phi_{t_0}^t(\mathbf{y})\right\|}{\|\mathbf{y}\|}\right), \tag{7}$$

where $\mathbf{y}$ is a small perturbation in the tangent space at x [28]. One can use the expression above on non-Euclidean manifolds and to derive an algorithm for computing FTLE on an unstructured mesh (for Euclidean or non-Euclidean manifolds). For Euclidean manifolds (e.g., $\mathbb{R}^n$), this expression reduces to,

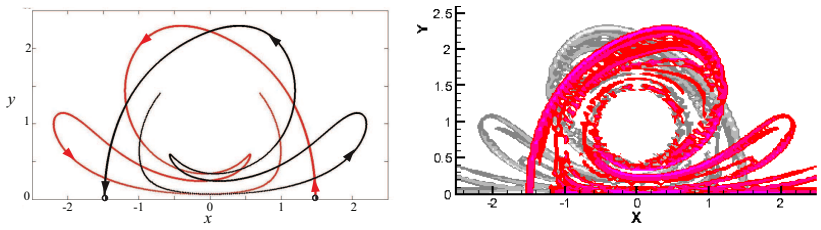

(a) (b)

Fig. 11 Comparison of FTLE-LCS and invariant manifolds in oscillating vortex pair flow (a) Unstable (red) and stable (black) manifolds of the two fixed points near $(\pm 1.5, 0)$ for the system parameters $(\gamma, \varepsilon) = (0.5, 0.1)$. See [83] for details. (b) FTLE-based LCS for the same system parameters. Notice that the ridge of high forward ($T > 0$) FTLE (red), the repelling LCS, corresponds with the stable manifold of the left fixed point of (a), and similarly for the high backward ($T < 0$) FTLE (gray, the attracting LCS, which corresponds with the unstable manifold of the right fixed point of (a). Computations by Shibabrat Naik.

$$\sigma(x, t_0, t) = \frac{1}{|t - t_0|} \log\left(\sqrt{\lambda_{max}(C(x, t_0, t))}\right), \tag{8}$$

where $C(x, t_0, t) = \left(\frac{d\phi_{t_0}^t}{dx}\right)^* \left(\frac{d\phi_{t_0}^t}{dx}\right)$ is the Cauchy-Green tensor, * denotes transpose, and $\lambda_{max}(A)$ denotes the maximum eigenvalue of matrix A

FTLE-LCS as Finite-Time Analogues of Stable and Unstable Manifolds. The FTLE at x measures the maximum stretching rate over the interval $T = t - t_0$ of trajectories starting near the point x at time t_0 [35]. Ridges of high $\sigma(x, t_0, t)$ correspond to surfaces of co-dimension one, meaning they separate qualitatively different regions of flow. Repelling (attracting) LCS for $T > 0$ ($T < 0$) are the *time-dependent generalizations of stable (unstable) manifolds* of NHIMs. Consider the model of fluid particles in the presence of an oscillating vortex pair [83], a flow induced by two counter rotating vortex pairs of equal circulation. This is a time-periodic system, where the stroboscopic map has two saddle-type fixed points whose manifolds can be computed. We can compare these manifolds with the FTLE field.

Even in the absence of, e.g., saddle fixed points, one can use the analogy of repelling and attracting LCS as stable and unstable manifolds to discern transport structure. Transport occurs via alleyways bounded by undulating repelling and attracting LCS surfaces. An aperiodic version of heteroclinic-tangle chaos occurs where these surfaces intersect (see Fig. 10). One can consider finite-time aperiodic versions of lobe dynamics as governing phase space transport where heteroclinic or homoclinic-like intersections occur. A rich time-dependent interplay of structures is observed in geophysical systems [37], such as the atmosphere, oceans, and lakes, but much is still unknown.

For example, consider a homoclinic tangle observed in a hurricane as in Fig. 12. The storm shown is Andrea, the first storm of the 2007 hurricane season. Notice the outline of the U.S. east coast. One can tease out the geometry of entrainment of an

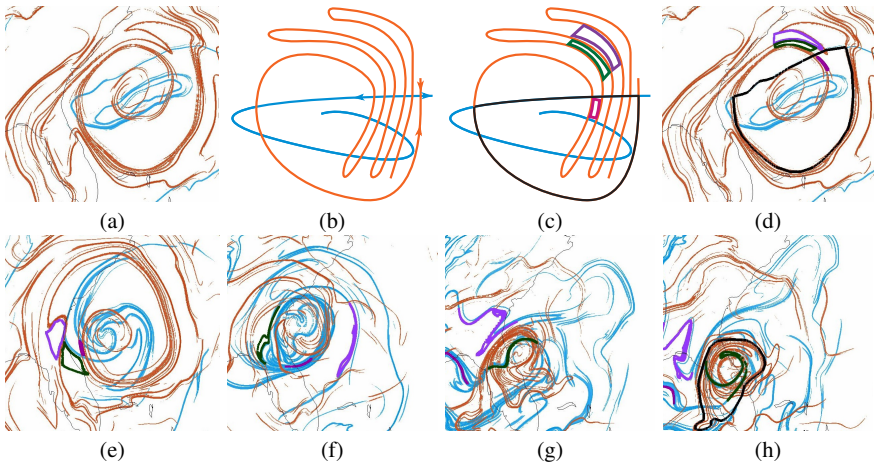

Fig. 12 Atmospheric LCS off the coast of Florida (coastal outline shown) for May 2007 computed from NOAA's NAM archive data at the 900mb pressure level. The trellis-like intersections of repelling [orange] and attracting [cyan] curves (a) form an object which behaves like a homoclinic tangle (shown in schematic, (b)). Coloring according to the dictates of lobe dynamics (schematic, (c) and actual, (d)), the green tile will get entrained, while the purple and magenta tiles will remain, or be removed, outside the main vortex defined by the moving separatrix (highlighted in black). As time progresses ((e) through (h)), we see that the theory's predictions hold, a consequence of the geometry of intersections. For reference, the separatrix boundary of the storm's vortex is shown again in the final panel, (h).

air mass into a hurricane's vortex (and detrainment out of the vortex). A separatrix, defining the boundary of the storm's vortex, is first determined from intersections of the repelling and attracting curves (to give an 'inside' and 'outside'). Parcels are labeled according to lobe dynamics theory, and as time progresses, the parcels perform lobe dynamics predicts. The green parcel, currently outside, should get entrained. Right next to it, but on the other side of a repelling curve, is a light pink region which should remain outside. Also, the dark magenta region inside will get detrained out of the vortex. The theory of homoclinic tangles was originally developed for time-independent or time-periodic systems, but seems to work even in this turbulent, aperiodic setting. This is remarkable, since there is no actual saddle-type fixed point with which to associated the 'stable' and 'unstable' manifolds. Rather, a distinguished repelling and attracting LCS intersection point behaves as a saddle point for the purposes of the theory.

2.4 Set-Oriented Approach, Alternate FTLE Definition, and Coherent Sets

A complementary method for computing transport uses almost-invariant sets (AIS), strongly connected (almost-invariant) regions computed via an operator-theoretic approach [18, 24, 56]. AISs are defined for autonomous and time-periodic systems, but for more general time dependence, we consider coherent sets, which generalize AISs [84]. In a partition of the phase space into subsets, LCS play the role of separatrices, but coherent sets play the role of the subsets they separate; coherent sets and LCS are therefore dual structures.

Perron-Frobenius Operator and Box Discretization of Phase Space. Let μ denote the Lebesgue measure on $M \subset \mathbb{R}^n$ and $\phi(x)_{t_0}^t : M \times \mathbb{R} \times \mathbb{R} \to M$ be a flow map on M from time t_0 to t. Let B be a measurable set and $f \in L^1(M)$ be a probability density function, $L^1(M)$ being the space of Lebesgue measurable functions on M. The unique operator $\mathbb{P}_{t_0}^t : L^1(M) \mapsto L^1(M)$ defined by

$$\int_B \mathbb{P}_{t_0}^t f d\mu = \int_{(\phi_{t_0}^t)^{-1}(B)} f d\mu \tag{9}$$

is called the Perron-Frobenius operator for the flow $\phi_{t_0}^t$, [85]. Equation (9), which holds for all μ measurable sets, follows from the Radon-Nykodym theorem.

In practice it is usually necessary to numerically approximate the operator $\mathbb{P}_{t_0}^t$. This is done by discretizing the domain, M, into a finite number of sets, say $\{B_1, B_2, ..., B_n\}$ which is essentially a grid of boxes, the disjoint union of which is M, i.e., $M = \bigcup_i B_i$. A projection $\pi : L^1(M) \mapsto \text{span}\{B_1, ..., B_n\}$ defined by $\pi f = \sum_{i=1}^n c_i \mathbb{X}_{B_i}$, where $\mathbb{X}_{B_i}$ is the characteristic function of the set B_i and $c_i = \frac{\int f d\mu}{\mu(B_i)}$ gives a finite dimensional approximation of f. Since f is a probability density function, $c_i = \frac{1}{\mu(B_i)}$. Similarly, $\mathbb{P}_{t_0}^t f$ is projected on span$\{B_1, ..., B_n\}$. The operator $P_{t_0}^t : \pi f \mapsto \pi \mathbb{P}_{t_0}^t f$ is a linear operator between finite dimensional vector spaces. Further taking the box measures $\mu(B_i) = \mu(B_j)$ for all $i, j \in \{1, \ldots, n\}$, $P_{t_0}^t$ becomes a stochastic transition matrix. The entries of the matrix P are determined by a Monte-Carlo simulation [17, 86]. Each box in the domain contains a fixed number of points (initial conditions) which are integrated from a time t_0 to t. The final position of the points gives the matrix P as,

$$(P_{t_0}^t)_{ij} = \frac{\mu(B_i \cap (\phi_{t_0}^t)^{-1}(B_j))}{\mu(B_j)}. \tag{10}$$

See Fig. 13 for a geometric interpretation. A time-reversible operator P is required to apply the above definition for flows in forward time [86]. This is achieved by creating a reversible Markov operator P_r given by

$$(P_{t_0}^t)_r = \frac{(P_{t_0}^t) + \overline{(P_{t_0}^t)}}{2} \tag{11}$$

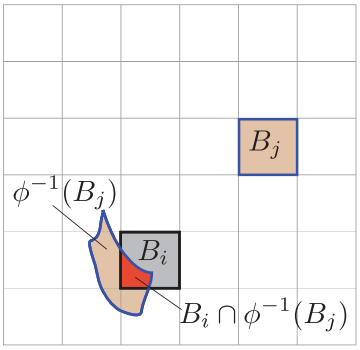

Fig. 13 Box-discretization method to calculate P. Box B_j at the final time t is mapped (backwards) to $\phi^{-1}(B_j)$ at the initial time t_0. The value of the entry P_{ij} is the fraction of box B_i that is mapped into box B_j by ϕ. Note that $\sum_{j=1}^{n} P_{ij} = 1$.

where $\overline{P}$ is the time reversed analogue of P. Its elements are given by

$$(\overline{P^t_{t_0}})_{ij} = \frac{u_{1j}(P^t_{t_0})_{ji}}{u_{1i}} \tag{12}$$

where u_{1j} and u_{1i} are components of the first left eigenvector, u_1, of $P^t_{t_0}$. For a volume preserving flow in which the domain is uniformly discretized, $\overline{P^t_{t_0}} = (P^t_{t_0})^*$, the transpose of $P^t_{t_0}$. Henceforth for convenience the time reversible operator $(P^t_{t_0})_r$ is referred to simply as P unless there is an ambiguity about the initial and final times t_0 and t. The Markov operator P has the semigroup property of $P^t_{t_0} = P^s_{t_0} P^t_s$, where $s \in (t_0, t)$.

Almost-Invariant Sets. A probability density function f is invariant under the flow if and only if f is a fixed point of P, i.e., $f = Pf$ [85]. The associated measure μ_f is called the invariant measure of the flow [24]. If the flow $\phi^t_{t_0}$ is volume preserving then the highest eigenvalue of P is always 1. This means that the entire domain M maps back onto itself. We make the additional observation that from (9), it follows that if $f > 0$, then $Pf > 0$. A set $B \in \mathbb{B}$ is considered *almost-invariant* over the interval $[t_0, t]$ if

$$\rho_{\mu_f}(B) = \frac{\mu_f(B \cap (\phi^t_{t_0})^{-1}(B))}{\mu_f(B)} \approx 1. \tag{13}$$

One can in theory construct an optimization problem to maximize the value of ρ_{μ_f} over all possible combinations of sets $B \in \mathbb{B}$. But this problem is combinatorially hard to solve even for simple flows. Therefore heuristic methods advanced in [17, 86] are adopted to identify maximally AISs. It was shown in [17, 86, 87] that the left eigenvector corresponding to the second eigenvalue gives the 'second most' almost-invariant sets, the invariance being higher if the second eigenvalue of P is closer to 1, with

$$\rho_{\mu_f}(B) = \frac{\sum_{i,j} u_j P_{ji}}{\sum_j u_j}. \tag{14}$$

For computational reasons we will make use of the singular vectors of P_r instead of the eigenvectors as was done in [88]. This is because the singular value

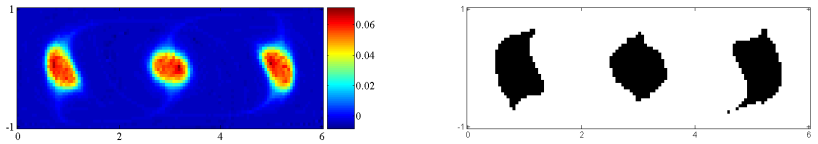

(a) (b)

Fig. 14 (a) Second eigenvector U_2^* for the lid-driven cavity flow and (b) AIS obtained from positive part of the second eigenvector of P, in black (composed of three disconnected sets, which in this case are almost-cyclic sets of period 3). The phase space complement, in white, is also an AIS. Details in [84].

decomposition is well conditioned and less sensitive to small changes in the matrix P_r introduced due to the discretization. It should be noted that P_r is self-adjoint and normal since $P_r = \frac{1}{2}(P + P^*) = P_r^*$ and $P_r^* P_r = P_r P_r^*$. From the spectral theorem, P_r has a unitary eigen-decomposition and the left eigenvectors of P_r are given by

$$P_r = Y^* \Lambda Y \tag{15}$$

with $Y^* = Y^{-1}$. P_r also has a unique singular value decomposition given by $P_r = U\Sigma V^* = P_r^* = V\Sigma U^*$ and $Y = U$, i.e., the left singular vectors and left eigenvectors of P_r are the same.

We note that the singular vectors U^* form an orthonormal basis for P_r. The first singular vector U_1^*, associated with the singular value 1, is the stationary distribution and is positive. Since $U_2^* \perp U_1^*$ we can infer that U_2^* has both positive and negative parts. From the definition of a Markov operator, $P_r(U_2^*)^+ > 0$ and $P_r(U_2^*)^- < 0$. So the sets on which the positive and negative parts of the second singular vector U_2^* are supported are AISs and partition the domain M into two parts. A 2-dimensional example from a periodic fluid velocity field in fluid mechanics is given Fig. 14, showing the vector U_2^* and the AISs.

Agreement Between AIS-Based and Lobe Dynamics-Based Transport Calculations. We note that in an autonomous setting, regions defined by the lobe dynamics approach are often AISs defined using the method described above. And the rates of transport determined by the two methods—lobe areas and AIS 'leakiness', respectively—are also in agreement [18], showing that, at least for autonomous or periodic systems, the geometric and probabilistic approaches are in agreement.

Coherent Sets for Systems of Arbitrary Time-Dependence. In autonomous systems an important feature of AISs is that they identify sets that mix minimally with the rest of the domain. Many time-dependent systems of practical interest may not have AISs. Moreover, systems defined by numerical data may be defined over leaky domains. In these cases, the approximation of the Perron-Frobenius operator by a stochastic transition matrix becomes difficult.

To extend the concept of AIS to time dependent systems we make the observation that AISs are also sets that stretch and deform minimally. Coherent sets—the time dependent analogues of AISs—can be defined as sets that do not mix significantly

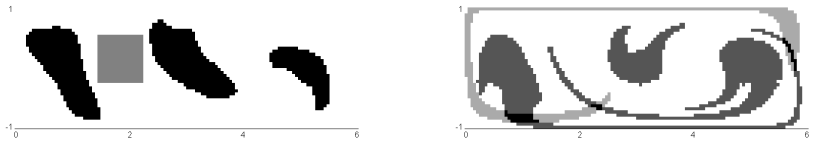

(a) $t = 0$ (b) $t = \tau_f$

Fig. 15 Coherent sets (black) do not disperse significantly while non coherent sets (gray) do. In (a) the three coherent sets (black) identified by our $\sigma_I \leq 0.06$ criterion and a non-coherent set (gray) are shown at $t = 0$. At t equal to one period of the fluid velocity field, τ_f, the non-coherent set disperses significantly more than the coherent sets. Notice that the three coherent sets are similar to the three-components of the AIS in Fig. 14. In (b), mixing between the 'particles' of the non-coherent set with those of the coherent sets is shown.

with the rest of the domain. This can be made more precise by first defining a set oriented FTLE. To make the discussion more concrete we initially define the FTLE for two dimensional systems.

Consider a uniform probability density function supported on a set B given by, $f = \frac{1}{\mu(B)}\mathbb{X}_B$, where $\mathbb{X}_B$ is characteristic function of B. The covariance matrix of f is $I_{ij} = E[(X_i - \overline{X}_i)(X_j - \overline{X}_j)]$, with $i, j = \{1, \ldots, n\}$ where $(\overline{X}_1, \ldots, \overline{X}_n)$ is the mean value of the random vector X and $E[\,\cdot\,]$ denotes the expected value. Under the action of the flow $\phi_{t_0}^t$, f is mapped to $\mathbb{P}_{t_0}^t f$ where $\mathbb{P}_{t_0}^t$ is the associated Perron-Frobenius operator. Let $I(f)$ be the covariance of f and $I(\mathbb{P}f)$ the covariance of $\mathbb{P}f$. Then the FTLE of B denoted by $\sigma_I(B, t_0, t)$ is defined as

$$\sigma_I(B, t_0, t) = \frac{1}{|t - t_0|} \log \left(\frac{\sqrt{\lambda_{max}(I(\mathbb{P}f))}}{\sqrt{\lambda_{max}(I(f))}} \right). \tag{16}$$

It can be shown by direct calculation that the covariance FTLE obtained from this definition and the standard FTLE definition (8) have the same value, i.e., $\sigma_I(B, t_0, t)$ converges to $\sigma(x, t_0, t)$ in the limit where B converges to a point x. But the σ_I definition can apply to arbitrary sets, not just points.

A set B is almost-coherent during $[t_0, t]$ if $\sigma_I(B, t_0, t) \approx 0$. This definition of coherence captures the essential feature of a coherent set: it does not mix or spread significantly in the domain. This definition also can identify non-mixing translating sets. Coherent sets can be identified by setting a heuristic threshold, say $\sigma_I^{\max}$, and considering as coherent sets the regions where $\sigma_I \leq \sigma_I^{\max}$. The probabilistic techniques described in this section are illustrated by the example of a piecewise smooth periodic lid driven cavity flow, with period τ_f (described in [31]). The AISs are shown in Fig. 14 while the coherent sets for the same example are shown in Fig. 15. Notice the similarity for this case. The coherent set definition has the advantage that it is applicable to systems of arbitrary time dependence where coherent sets could be highly mobile.

As recently discovered [31], the space-time 'braiding structure' of almost-cyclic coherent sets can be analyzed using topological methods [52] to predict and quantify

chaotic transport in the surrounding fluid. Since these tools are based in topology, the overall space-time structure of their interactions determines the transport predictions without requiring highly-resolved dynamical information. The merging of coherent sets and topological perspectives has great potential for making quantitative predictions of global transport with limited information.

3 Exploiting Chaotic Transport for Efficient Movement

Natural environmental fluid flows, such as those found in the atmosphere, oceans, lakes, and ground water, exhibit complex dynamics. This complexity is actually a boon for transporting mobile quasi-passive agents. Rich, chaotic dynamical structure makes efficient movement and dispersal possible, whether the agents are biological, chemical, or engineered devices like sensor platforms and delivery vehicles that seek energy efficiency or stealth [89]. Exploiting (or preventing) this transport requires the ability to accurately and rapidly identify these complex dynamical structures and predict their future motion. Despite the flow complexity, preliminary work suggests that it is possible to discern the time-dependent transport network of dynamical structures that geometrically organize the motion over scales of interest in realistic flows, e.g., Fig. 10. However, substantial work remains to be done to develop the underlying dynamical systems theory, connect these mathematical structures with experimental data, and implement efficient computation and prediction of observed structures.

3.1 Using Invariant Manifolds and their Time-Dependent Analogs in Efficient Control Strategies

Understanding the time-varying structures governing transport is important for advanced prediction (and control) of natural processes, but can also be exploited for engineered systems; agents navigating using invariant manifolds of saddle points (or NHIMs) or LCSs (in the case of data-based, time-aperiodic flows) can easily switch from one region of interest to another with minimal energy expenditure. Consider the schematic example of Fig. 16, where small controls can steer an agent into subregions which travel to desired destinations, which would not be reachable by a direct route.

Compared with conventional control methods that use only local information, incorporating global information opens new possibilities. The techniques to achieve this are a critical step in a long term vision to control multiple weakly propelled agents in 3D time-chaotic flows, in which the goal is to cooperate to achieve an overall group objective such as surveillance, search and rescue, exploration, or improved data collection or flow prediction.

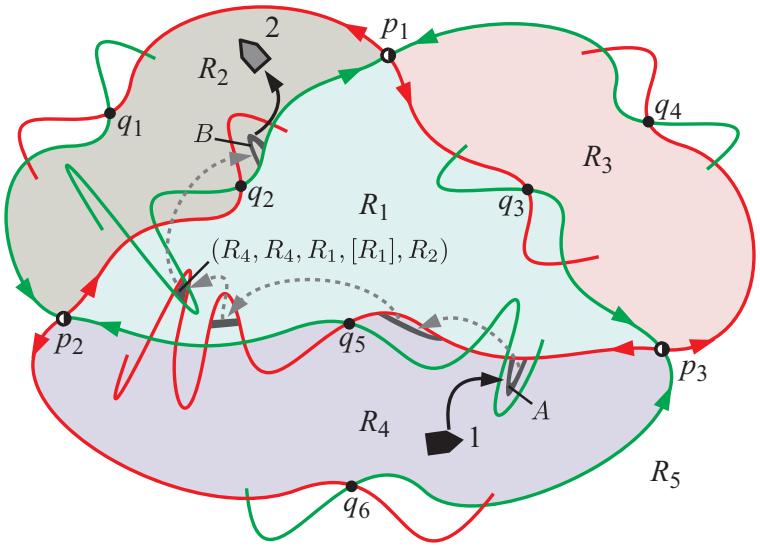

Fig. 16 The same regions as given in Fig. 6 are redrawn. A weakly propelled mobile agent initially at position 1 in region R_4 has an objective or reaching a target position 2 in region R_2, but a direct route is not possible given control limitations. The agent therefore follows a strategy of taking advantage of the existing flow structure, using a small control to enter subregion A. Under the evolution of the system (e.g., consider we have a period-T flow viewed via a time-T map), after several periods the subregion has evolved without control into B in region R_2, where a small control can take the agent to the desired position.

The use of natural lanes of transport bounded by LCS has been extensively developed in control strategies for interplanetary spacecraft trajectory design, where in this setting the LCS are the stable and unstable manifolds of NHIMs (see [47, 51] and references therein). In this application, on-board fuel is a premium, therefore the goal is to find fuel-efficient paths which lead to, for example, an orbit around a moon of Jupiter. Although the flow field for a spacecraft lives in a six dimensional phase space—three dimensions of position and three dimensions for velocity—the computation of LCS is straightforward. The LCS reveal gravitational sweet spots that provide natural gateways to destinations. Harnessing this effect to good purpose, mission designers can plan fuel-efficient routes, ones that would not otherwise be imaginable or technically feasible.

Theoretically, LCS are expected to reveal natural fuel-free or low-fuel dynamical channels for spacecraft even in a time-dependent gravitational field [90]. This has been demonstrated numerically, where for the time-dependent flow field, the LCS are typically time-dependent surfaces [69, 70, 73, 91]. Targeting of LCS for spacecraft control has been demonstrated to reveal near optimal trajectories even in the presence of navigation or control errors [92].

Although a different setting, LCS have also been shown to approximate fuel-optimal paths for underwater gliders in coastal waters [93]. The approximately two-dimensional near-surface ocean flow is obtained from observational data and reveals

rich dynamical structure with discernible features despite the time-chaotic dependence of the flow.

3.2 Control Strategies for Weakly Propelled Vehicles in Complex Environmental Flows

LCS- and AIS- or coherent set-based control can provide deployment and station-keeping where other control schemes fail, particularly for quasi-passive agents with velocities that are significantly lower than that of the environmental flow velocity [94]. We contend that vehicles (whether nano-, micro- or macro-scale) with limited power and control authority can similarly exploit a complex environmental flow for efficient transport when motion planning is informed by the evolving structures identified in the flow.

Controllability and Accessibility. Fundamental to motion planning in a time-varying flow is the question of *controllability* on a given time interval: Is there a controlled trajectory connecting *arbitrary* initial and final states? For a weakly propelled agent in a significant flow, the answer will be "no," but the system may be *accessible* in the sense that the reachable subspace is non-empty. Thus, one must ask: Does the reachable subspace contain a point or region of interest? And, if so: What control history is required? While there are well-developed notions of controllability and accessibility for nonlinear time-varying systems, constructive results (i.e., control design methods) exist only in special cases where the system exhibits an underlying structure that can be exploited to simplify analysis. For drift-free, time-invariant systems, for example, controllability can be tested using the Lie algebra rank condition [95, 96]. Having verified controllability, one may generate a time-varying input history, perhaps constructed from a library of "motion primitives," to achieve a control objective. Of course, controllability for systems with drift is more challenging.

In cases of interest to us, the primary source of drift will be the ambient flow field, which will break any natural symmetries that might otherwise be exploited in controllability analysis. Moreover, because environmental drift will *dominate* the dynamics of a weakly propelled agent, the dynamics will be accessible, at best, with severe implications for motion planning. Some key theoretical questions arise. What is the appropriate notion of accessibility for a weakly propelled agent in a time-varying flow that is characterized by LCS or coherent sets and how does one assess this property? Can structural properties of LCS or coherent sets be exploited to simplify the computations required to evaluate accessibility and characterize the reachable subspace?

To answer these questions, one must cast the control objective (e.g., waypoint following, area or volume coverage, etc.) in terms of the reachable subspaces for individual agents, given the flow field structure. Accessibility will be tied to predictions of the time-varying flow and dynamical structures. One must therefore con-

sider a tradeoff between potential benefits of a long planning horizon (e.g., transport economy) and uncertainty in the model prediction.

Optimal Locomotion in Flows. Having developed machinery to evaluate accessibility and characterize the reachable subspace, one may then consider motion planning. What is the most energy-efficient path from point A to point B? What path from point A to point B maximizes the reachable subspace in the terminal phase? Given an initial distribution of weakly propelled agents, what collection of paths maximizes information gain (concerning the flow itself, some airborne constituent, some object on the ground, or any other measurable quantity of interest)? The first of these questions has been considered in some detail for kinematic vehicle models in planar, constant-relative-speed motion where the flow field is steady and uniform. For a kinematic particle model with turn rate constraints, for example, there are geometric path planning strategies that concatenate maximum effort and singular arcs to create minimum-time paths [97, 98]. Turn acceleration constraints are considered in [99]. While these methods exploit (or mitigate) the effects of the ambient flow, the vehicles are "strongly propelled" and the "structure" of the flow is trivial, such as a cellular flow. We ask whether, in the more challenging conditions of a time-varying, flow field, the structural properties of LCS or coherent sets can be exploited to obtain simple, effective motion planning and control strategies for weakly propelled vehicles.

A Conceptual Example. Suppose we have a fully actuated mobile agent and we consider only translational dynamics. For simplicity of discussion, we assume that the agent is a point of unit mass. We can also suppose that there fixed obstacles to be avoided. This will lay a foundation for more detailed future studies considering the effects on a finite-size body or vehicle [100], with perhaps biologically-inspired shape change actuation [101] where coupling of translational with rotational motion is critical.

We desire a feedback control law to (asymptotically) drive the agent to a target point x_T in a target region, which may have dynamics of its own, e.g., a point on or near an LCS curve (Fig. 17(b)). A detection shell, a ball of radius r_{det}, is given to the agent such that the agent can respond to any feature within this shell, such as an LCS curve that its desirable to follow.

The agent's equation of motion are given by

$$\dot{x} = v_{\text{f}}(x,t) + v_{\text{r}} \qquad \text{and} \qquad \dot{v}_{\text{r}} = u. \tag{17}$$

Subscripts indicate that terms pertain to the flow ("f") and flow-relative motion ("r") due to control. The objective in this example is to drive an agent asymptotically to a target point x_T in a target region, which may have dynamics of its own, e.g., a point on or near an LCS curve (Fig. 17(a)). We are interested in the weakly propelled or *quasi-passive case* where $\|v_{\text{f}}\| < \|v_{\text{r}}\|$, where knowledge of the geometry of flow structures is critical to motion planning. Assigned to the agent is a detection shell, a ball of radius r_{det}, within which the agent may respond to flow features such as an LCS curve that might be followed toward the target. Inspired by recent devel-

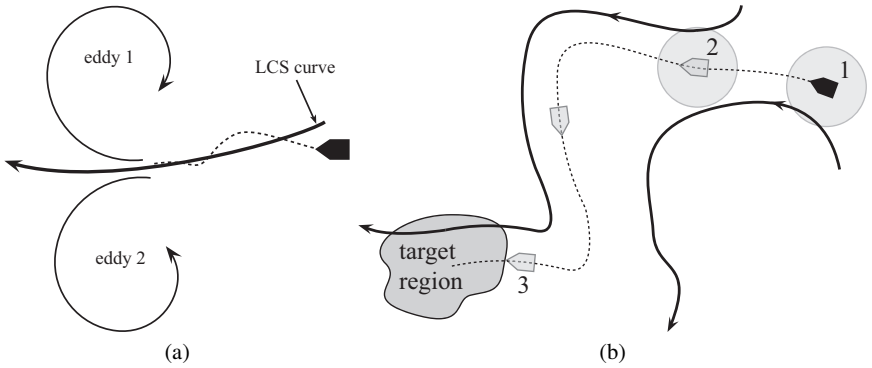

Fig. 17 (a) Straddling an LCS to easily switch between two dynamically distinct regions, for instance, two eddies. (b) The mobile agent follows the nearest LCS curve which is within a detection shell, shown schematically at position 1. At position 2, the agent switches to another curve, finally reaching the target region at 3. The arrows on the LCS curves denote the motion along them. Although not shown in this schematic, the LCS curves have dynamics of their own and will move.

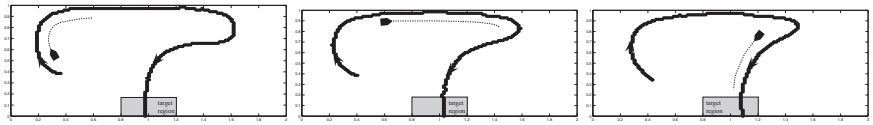

Fig. 18 A vehicle in a simple model of a perturbed double-gyre flow is shown at three successive times. The vehicle is using small control to take best advantage of the flow to reach the target region by following an LCS curve. The evolution of the LCS is visible as well as the short-time estimate of the vehicle's future trajectory. See [94] for details.

opments in reactive collision avoidance [102], the agent might employ a feedback control law $u = F_p + F_g + F_d$ comprising an error potential force $F_p = -\nabla V(x)$, a gyroscopic steering force F_g, and a damping force F_d. Rather than plan an explicit path based on a flow field estimate, the agent may simply react to the evolving ambient flow conditions as they are encountered.

These forces can be chosen to illustrate three motion control methods that exploit an environmental flow characterized by an coherent set or LCSs:

1. Straddling an LCS for easy movement between dynamically distinct regions (AIS or coherent sets): We consider the target point x_T to be on an LCS, moving just ahead of the agent as in Fig. 17(a). One suitable potential function is a quadratic function of the distance to the target $V(x) = \frac{1}{2}||x - x_T||^2$.
2. Following an efficient navigation pathway bounded by time-varying LCS surfaces (i.e., within an evolving coherent set) to reach a target region: We use a form of the gyroscopic force appropriate for tracking a smooth boundary [103]. If more than one LCS surface is within the agent's detection shell, the agent only reacts to the closest one, as in Fig. 17(b).

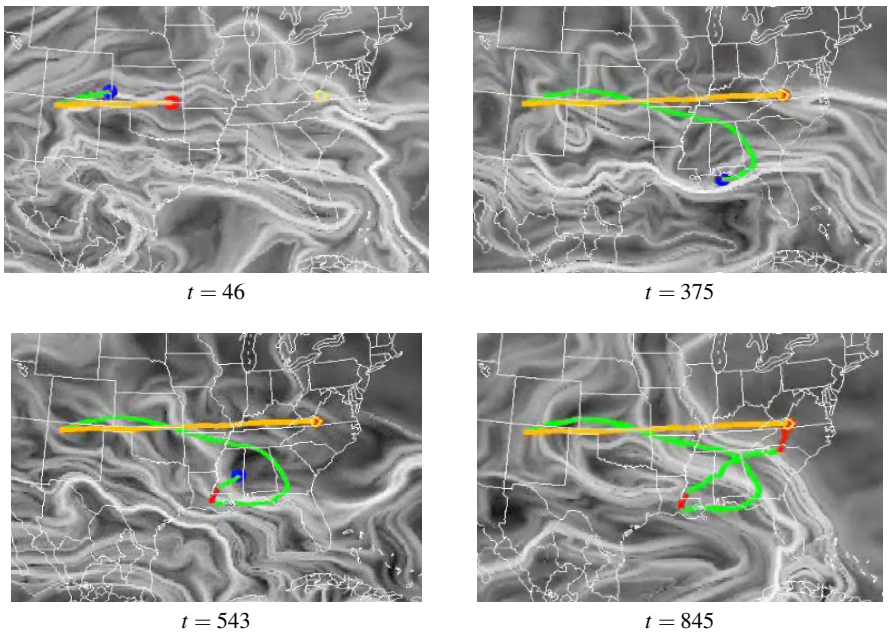

Fig. 19 Two aerial vehicles are experiencing atmospheric flow. Although starting and ending at the same points, a strongly propelled high speed vehicle (straight line) uses much more energy than a weakly propelled quasi-passive vehicle that 'jumps' over LCS from one coherent set to another as needed to reach the target. The background grayscale field is the time-varying FTLE field; darker regions are more coherent, separated by ridges (LCS). The weakly propelled vehicle agent moves passively along a coherent set from $t = 0$ to around $t = 400$, when it starts heading in the wrong direction. So the vehicle applies a little control to jump over an LCS into a different coherent set heading in the right direction, with some fine control near the end to reach the target. Continental and political boundaries are shown to provide scale. Computations by Carmine Senatore.

3. Leap-frogging coherent sets to reach a destination: Passively following a coherent set while it heads in the general direction of the target region and when it veers away, selectively "jumping over" LCS to neighboring coherent sets which are headed in the right direction. This strategy views the environmental flow as an ever-changing system of "conveyor belts" moving in different directions.

The proposed strategies will quickly determine near energy-optimal trajectories: an example of strategy 2 is shown in Fig. 18 for a vehicle in a perturbed double-gyre flow [94]. A more realistic example in a high-fidelity atmospheric flow over the U.S. is shown in Fig. 19, displaying option 3. For any numerical optimal control algorithm, a good initial guess is vital, especially if the problem is very sensitive numerically. By having good approximate paths "built in" to the algorithms via LCS, the above control strategies will initialize any optimization strategy closer to the true optimum path. We hypothesize that this will also hold if one considers the situation where LCS can only be determined from approximate forecasts—for instance, LCS from model forecasts or assumptions on the evolution of the LCS

themselves up to some finite-time horizon. One can also consider that for different motion models, generalized hyperbolic surfaces will emerge. That is, different models and controls give rise to different flow maps and thus additional generalizations of LCS which may be important for motion planning.

4 Conclusions

Several geometric and probabilistic methods for studying chaotic phase space transport have been developed and fruitfully applied to diverse areas from orbital mechanics to biomechanics to fluid mechanics and beyond. Increasingly, systems of interest are determined not by analytically defined model systems, but by data from experiments or large-scale simulations. We have discussed those features of phase space transport in finite-time systems which seem to be robust, considering invariant manifolds and invariant manifold-like objects, and their connection with concepts such as symbolic dynamics, almost-invariant sets, and coherent sets.

The methods outlined above provide the mathematical and computational tools necessary to identify and track dynamical structures (i.e., LCS and coherent sets) in multi-dimensional, time-dependent, complex flows in abstract phase spaces. When the focus is on fluid flows, the presence and prediction of these dynamical structures in realistic fluid flows can be exploited to achieve efficient transport of vehicles with limited power and control authority. These methods may even provide insight into the movement of weakly propelled agents in biological contexts, such as jellyfish or rays in the oceans, airborne pathogens in the atmosphere [89], or internal physiological flows.

Acknowledgements We wish to thank Carmine Senatore and Shibabrat Naik for contributing their computations. This material is based upon work supported by the National Science Foundation under Grant Nos. 0919088, 0938047 and 1100263. Any opinions, findings, and conclusions or recommendations expressed in this material are those of the authors and do not necessarily reflect the views of the National Science Foundation.

References

[1] Koon, W. S., Lo, M. W., Marsden, J. E. and Ross, S. D. [2000] Heteroclinic connections between periodic orbits and resonance transitions in celestial mechanics. *Chaos* **10**:427–469.

[2] Gabern, F., Koon, W. S., Marsden, J. E. and Ross, S. D. [2005] Theory and Computation of Non-RRKM Lifetime Distributions and Rates in Chemical Systems with Three or More Degrees of Freedom. *Physica D* **211**:391–406.

[3] Gabern, F., Koon, W. S., Marsden, J. E., Ross, S. D. and Yanao, T. [2006] Application of tube dynamics to non-statistical reaction processes. *Few-Body Systems* **38**:167–172.

[4] Jaffé, C., Farrelly, D. and Uzer, T. [1999] Transition state in atomic physics. *Phys. Rev. A* **60**:3833–3850.

[5] Jaffé, C., Farrelly, D. and Uzer, T. [2000] Transition state theory without time-reversal symmetry: chaotic ionization of the hydrogen atom. *Phys. Rev. Lett.* **84**:610–613.
[6] Martens, C. C., Davis, M. J. and Ezra, G. S. [1987] Local frequency analysis of chaotic motion in multidimensional systems: energy transport and bottlenecks in planar OCS. *Chem. Phys. Lett.* **142**:519–528.
[7] De Leon, N. [1992] Cylindrical manifolds and reactive island kinetic theory in the time domain. *J. Chem. Phys.* **96**:285–297.
[8] De Leon, N. and Ling, S. [1994] Simplification of the transition state concept in reactive island theory: Application to the HCN=CNH isomerization. *J. Chem. Phys.* **101**:4790–4802.
[9] De Leon, N., Mehta, M. A. and Topper, R. Q. [1991] Cylindrical manifolds in phase space as mediators of chemical reaction dynamics and kinetics. I. Theory. *J. Chem. Phys.* **94**:8310–8328.
[10] De Leon, N., Mehta, M. A. and Topper, R. Q. [1991] Cylindrical manifolds in phase space as mediators of chemical reaction dynamics and kinetics. II. Numerical considerations and applications to models with two degrees of freedom. *J. Chem. Phys.* **94**:8329–8341.
[11] Shadden, S. C., Lekien, F. and Marsden, J. [2005] Definition and properties of Lagrangian coherent structures from finite-time Lyapunov exponents in two-dimensional aperiodic flows. *Physica D* **212**:271–304.
[12] Lekien, F., Shadden, S. C. and Marsden, J. [2007] Lagrangian coherent structures in n-dimensional systems. *Journal of Mathematical Physics* **48**.
[13] Wiggins, S. [1993] *Chaotic transport in dynamical systems, Interdisciplinary Applied Mathematics*. Springer, first edn.
[14] Ide, K., Small, D. and Wiggins., S. [2002] Distinguished hyperbolic trajectories in time dependent fluid flows: Analytical and computational approach for velocity fields as data sets. *Nonlinear Processes in Geophysics* **9**:237–263.
[15] Wiggins., S. [2005] The dynamical systems approach to Lagrangian transport in oceanic flows. *Annual Review of Fluid Mechanics* **37**:295 – 328.
[16] Haller, G. [2001] Lagrangian coherent structures and the rate of strain in a partition of two-dimensional turbulence. *Physics of Fluids A* **13**:3368–3385.
[17] Dellnitz, M. and Junge, O. [1998] On the approximation of complicated dynamical behavior. *SIAM Journal on Numerical Analysis* **36**:491–515.
[18] Dellnitz, M., Junge, O., Koon, W. S., Lekien, F., Lo, M. W., Marsden, J. E., Padberg, K., Preis, R., Ross, S. D. and Thiere, B. [2005] Transport in dynamical astronomy and multibody problems. *Int. J. Bifurc. Chaos* **15**:699–727.
[19] Dellnitz, M., Junge, O., Lo, M. W., Marsden, J. E., Padberg, K., Preis, R., Ross, S. D. and Thiere, B. [2005] Transport of Mars-crossing asteroids from the quasi-Hilda region. *Physical Review Letters* **94**:231102.
[20] Froyland, G. and Dellnitz, M. [2009] Detecting and locating near optimal almost invariant sets and cycles. *SIAM Journal on Scientific Computing* **24**:1507–1523.
[21] Froyland, G., Lloyd, S. and Santitissadeekorn, N. [2010] Coherent sets for nonautonomous dynamical systems. *Physica D* **239**:1527–1541.
[22] Froyland, G., Santitissadeekorn, N. and Monahan, A. [2010] Transport in time-dependent dynamical systems : Finite time coherent sets. *Chaos* **20**:043116.
[23] Du Toit, P. C. [2010] *Transport and separatrices in time dependent flows*. PhD thesis, California Institute of Technology.
[24] Dellnitz, M., Hohmann, A., Junge, O. and Rumpf, M. [1997] Exploring invariant sets and invariant measures. *Chaos* **7**:221.
[25] Coulliette, C., Lekien, F., Paduan, J. D., Haller, G. and Marsden, J. [2007] Optimal pollution mitigation in monterey bay based on coastal radar data and nonlinear dynamics. *Environmental Science and Technology* **41**:6562–6572.
[26] Tallapragada, P. and Ross, S. D. [2008] Particle segregation by Stokes number for small neutrally buoyant spheres in a fluid. *Physical Review E* **78**.

[27] Haller, G. and Sapsis, T. [2008] Instabilities in the dynamics of neutrally buoyant particles. *Physics of fluids* **20**.

[28] Lekien, F. and Ross, S. D. [2010] The computation of finite-time Lyapunov exponents on unstructured meshes and for non-Euclidean manifolds. *Chaos* **20**:017505.

[29] Tang, W., Mathur, M., Haller, G., Hahn, D. C. and Ruggiero, F. H. [2010] Lagrangian coherent structures near a subtropical jet stream. *Journal Atmospheric Science* **67**:2307–2319.

[30] Wilson, M., Peng, J., Dabiri, J. O. and Eldredge, J. D. [2009] Lagrangian coherent structures in low Reynolds number swimming. *Journal of Physics: Condensed Matter* **21**:204105.

[31] Stremler, M. A., Ross, S. D., Grover, P. and Kumar, P. [2011] Topological chaos and periodic braiding of almost-cyclic sets. *Physical Review Letters* **106**:114101.

[32] Cross, M. C. and Hohenberg, P. C. [1993] Pattern formation outside of equilibrium. *Rev. Mod. Phys.* **65**(3):851.

[33] Pierrehumbert, R. T. [1991] Chaotic mixing of tracer and vorticity by modulated traveling Rossby waves. *Geophys. Astrophys. Fluid Dyn.* **58**:285–319.

[34] Pierrehumbert, R. T. [1991] Large-scale horizontal mixing in planetary atmospheres. *Phys. Fluids A* **3**:1250–1260.

[35] Shadden, S. C., Lekien, F. and Marsden, J. E. [2005] Definition and properties of Lagrangian coherent structures: mixing and transport in two-dimensional aperiodic flows. *Physica D* **212**:271–304.

[36] Haynes, P. [2005] Stratospheric Dynamics. *Annu. Rev. Fluid Mech.* **37**:263–293.

[37] Du Toit, P. C. and Marsden, J. E. [2010] Horseshoes in hurricanes. *Journal of Fixed Point Theory and Applications* **7**(2):351–384.

[38] Dingwell, J. B. and Cusumano, J. P. [2000] Nonlinear time series analysis of normal and pathological human walking. *Chaos* **10**(4):848–863.

[39] Dingwell, J. B. [2006] Lyapunov exponent. In *The Wiley Encyclopedia of Biomedical Engineering* (edited by M. Akay). Wiley, New York.

[40] England, S. and Granata, K. P. [2007] The influence of gait speed on local dynamic stability of walking. *Gait & Posture* **25**:172–178.

[41] Tanaka, M. L. and Ross, S. D. [2009] Separatrices and basins of stability from time series data: an application to biodynamics. *Nonlinear Dynamics* **58**(1-2):1–21.

[42] Tanaka, M. L., Nussbaum, M. A. and Ross, S. D. [2009] Evaluation of the threshold of stability for the human spine. *Journal of Biomechanics* **42**(8):1017 – 1022.

[43] Tanaka, M. L., Ross, S. D. and Nussbaum, M. [2010] Mathematical modeling and simulation of seated stability. *Journal of Biomechanics* **43**:906–912.

[44] Ross, S. D., Tanaka, M. L. and Senatore, C. [2010] Detecting dynamical boundaries from kinematic data in biomechanics. *Chaos* **20**:017507.

[45] Tanaka, M. L. and Ross, S. D. [2011] Using topological equivalence to discover stable control parameters in biodynamic systems. *Computer Methods in Biomechanics and Biomedical Engineering* :to appear.

[46] Hénon, M. and Heiles, C. [1964] The applicability of the third integral of motion: some numerical experiments. *Astron. J.* **69**:73–79.

[47] Koon, W. S., Lo, M. W., Marsden, J. E. and Ross, S. D. [2008] *Dynamical Systems, the Three-Body Problem and Space Mission Design*. Marsden Books, ISBN 978-0-615-24095-4.

[48] Ross, S. D. [2006] The interplanetary transport network. *American Scientist* **94**:230–237.

[49] Ross, S. D. and Scheeres, D. J. [2007] Multiple gravity assists, capture, and escape in the restricted three-body problem. *SIAM Journal on Applied Dynamical Systems* **6**(3):576–596.

[50] Grover, P. and Ross, S. D. [2009] Designing trajectories in a planet-moon environment using the controlled Keplerian map. *Journal of Guidance, Control and Dynamics* **32**:436–443.

[51] Gawlik, E. S., Marsden, J. E., Du Toit, P. C. and Campagnola, S. [2009] Lagrangian coherent structures in the planar elliptic restricted three-body problem. *Celestial Mechanics and Dynamical Astronomy* **103**:227–249.

[52] Boyland, P. L., Aref, H. and Stremler, M. A. [2000] Topological fluid mechanics of stirring. *J. Fluid Mech.* **403**:227–304.

[53] Thiffeault, J.-L. and Finn, M. D. [2006] Topology, braids and mixing in fluids. *Phil. Trans. R. Soc. Lond. A* **364**(1849):3251–3266.
[54] Gouillart, E., Thiffeault, J. and Finn, M. [2006] Topological mixing with ghost rods. *Physical Review E* **73**(3).
[55] Stremler, M. A. and Chen, J. [2007] Generating topological chaos in lid-driven cavity flow. *Phys. Fluids* **19**:103602.
[56] Dellnitz, M. and Junge, O. [1999] On the approximation of complicated dynamical behavior. *SIAM Journal on Numeric Analysis* **36**:491–515.
[57] Jaffé, C., Ross, S. D., Lo, M. W., Marsden, J. E., Farrelly, D. and Uzer, T. [2002] Theory of asteroid escape rates. *Physical Review Letters* **89**:011101.
[58] Rom-Kedar, V. and Wiggins, S. [1990] Transport in two-dimensional maps. *Arch. Rat. Mech. Anal.* **109**:239–298.
[59] Rom-Kedar, V. and Wiggins, S. [1991] Transport in two-dimensional maps: Concepts, examples, and a comparison of the theory of Rom-Kedar and Wiggins with the Markov model of MacKay, Meiss, Ott, and Percival. *Physica D* **51**:248–266.
[60] Haller, G. and Yuan, G. [2000] Lagrangian coherent structures and mixing in two-dimensional turbulence. *Physica D* **147**:352–370.
[61] Haller, G. [2000] Finding finite-time invariant manifolds in two-dimensional velocity fields. *Chaos* **10**:99–108.
[62] Haller, G. [2001] Distinguished material surfaces and coherent structures in 3D fluid flows. *Physica D* **149**:248–277.
[63] Haller, G. [2001] Lagrangian structures and the rate of strain in a partition of two-dimensional turbulence. *Phys. Fluids* **13**:3365–3385.
[64] Haller, G. [2002] Lagrangian coherent structures from approximate velocity data. *Phys. Fluids* **14**:1851–1861.
[65] Lekien, F., Shadden, S. C. and Marsden, J. E. [2007] Lagrangian coherent structures in n-dimensional systems. *Journal of Mathematical Physics* **48**:065404.
[66] Bowman, K. P., Pan, L. L., Campos, T. and Gao, R. [2007] Observations of fine-scale transport structure in the upper troposphere from the High-performance Instrumented Airborne Platform for Environmental Research. *J. Geophys. Res.* **112**:D18111.
[67] Pan, L. L., Bowman, K. P., Atlas, E., Wofsy, S. C., Zhang, F., Bresch, J. F., Ridley, B. A., Pittman, J. V., Homeyer, C., Romashkin, P. and Cooper, W. A. [2010] The Stratosphere-Troposphere Analyses of Regional Transport 2008 (START08) Experiment. *Bull. Am. Meteorol. Soc.* **91**:D23102.
[68] Koon, W. S., Lo, M. W., Marsden, J. E. and Ross, S. D. [2001] Resonance and capture of Jupiter comets. *Celestial Mechanics and Dynamical Astronomy* **81**:27–38.
[69] Koon, W. S., Lo, M. W., Marsden, J. E. and Ross, S. D. [2001] Low energy transfer to the Moon. *Celestial Mechanics and Dynamical Astronomy* **81**:63–73.
[70] Koon, W. S., Lo, M. W., Marsden, J. E. and Ross, S. D. [2002] Constructing a low energy transfer between Jovian moons. *Contemporary Mathematics* **292**:129–145.
[71] Koon, W. S., Marsden, J. E., Ross, S. D., Lo, M. W. and Scheeres, D. J. [2004] Geometric mechanics and the dynamics of asteroid pairs. *Annals of the New York Academy of Sciences* **1017**:11–38.
[72] Ross, S. D. [2004] *Cylindrical manifolds and tube dynamics in the restricted three-body problem*. Ph.D. thesis, California Institute of Technology.
[73] Marsden, J. E. and Ross, S. D. [2006] New methods in celestial mechanics and mission design. *Bulletin of the American Mathematical Society* **43**:43–73.
[74] Newton, P. K. and Ross, S. D. [2006] Chaotic advection in the restricted four-vortex problem on a sphere. *Physica D* **223**:36–53.
[75] Jerg, S., Junge, O. and Ross, S. D. [2009] Optimal capture trajectories using multiple gravity assists. *Communications in Nonlinear Science and Numerical Simulation* **14**(12):4168 – 4175.

[76] Gómez, G., Koon, W. S., Lo, M. W., Marsden, J. E., Masdemont, J. and Ross, S. D. [2004] Connecting orbits and invariant manifolds in the spatial three-body problem. *Nonlinearity* **17**:1571–1606.

[77] Wiggins, S. [1992] *Chaotic Transport in Dynamical Systems*, vol. 2 of *Interdisciplinary Appl. Math.*. Springer, Berlin-Heidelberg-New York.

[78] Meiss, J. D. [1992] Symplectic maps, variational principles, and transport. *Rev. Mod. Phys.* **64**:795–848.

[79] MacKay, R. S., Meiss, J. D. and Percival, I. C. [1984] Transport in Hamiltonian systems. *Physica D* **13**:55–81.

[80] Schroer, C. G. and Ott, E. [1997] Targeting in Hamiltonian systems that have mixed regular/chaotic phase spaces. *Chaos* **7**:512–519.

[81] Tallapragada, P. and Ross, S. D. [2008] Particle segregation by Stokes number for small neutrally buoyant spheres in a fluid. *Physical Review E* **78**:036308.

[82] Senatore, C. and Ross, S. D. [2011] Detection and characterization of transport barriers in complex flows via ridge extraction of the finite time Lyapunov exponent field. *International Journal for Numerical Methods in Engineering* **86**:1163–1174.

[83] Rom-Kedar, V., Leonard, A. and Wiggins, S. [1990] An analytical study of transport, mixing and chaos in an unsteady vortical flow. *J. Fluid Mech.* **214**:347–394.

[84] Tallapragada, P. and Ross, S. D. [2011] A geometric and probabilistic description of coherent sets. *submitted* : .

[85] Lasota, A. and Mackey, M. C. [1994] *Chaos, Fractals and Noise. Stochastic Aspects of Dynamics*. Springer-Verlag, second edn.

[86] Froyland, G. and Dellnitz, M. [2003] Detecting and locating near-optimal almost-invariant sets and cycles. *SIAM Journal of Scientific Computing* **24**:1839–1863.

[87] Dellnitz, M. and Junge, O. [2002] Set oriented numerical methods for dynamical systems. In *Handbook of dynamical systems*, vol. 2, 221–264. North-Holland, Amsterdam.

[88] Fritzsche, D. and Mehrmann, V. [2006] An SVD approach to identifying metastable sets of Markov chains. *Technical Report, Institut fur Mathematik, Technishe Universitat Berlin* .

[89] Tallapragada, P., Ross, S. D. and Schmale, D. [2011]. Lagrangian coherent structures are associated with fluctuations in airborne microbial populations.

[90] Fenichel, N. [1971] Persistence and smoothness of invariant manifolds for flows. *Indiana University Mathematics Journal* **21**:193–226.

[91] Yamato, H. and Spencer, D. B. [2004] Transit-orbit search for planar restricted three-body problems with perturbations. *Journal of Guidance, Control, and Dynamics* **27**:1035–1045.

[92] Serban, R., Koon, W., Lo, M., Marsden, J., Petzold, L., Ross, S. D. and Wilson, R. [2002] Halo orbit mission correction maneuvers using optimal control. *Automatica* **38**:571–583.

[93] Inanc, T., Shadden, S. C. and Marsden, J. E. [2005] Optimal Trajectory Generation in Ocean Flows. In *Proceedings of 2005 American Control Conference*, 674–679.

[94] Senatore, C. and Ross, S. D. [2008] Fuel-efficient navigation in complex flows. In *Proceedings of 2008 American Control Conference*, 1244–1248.

[95] Nijmeijer, H. and van der Schaft, A. J. [1990] *Nonlinear Dynamical Control Systems*. Springer.

[96] Bloch, A. M. [2003] *Nonholomomic Mechanics and Control*. Applied Mathematical Sciences Series. Springer-Verlag.

[97] Techy, L. and Woolsey, C. A. [2009] Minimum-Time Path Planning for Unmanned Aerial Vehicles in Steady Uniform Winds. *Journal of Guidance, Control, and Dynamics* **32**(6):1736–1746.

[98] McGee, T. G. and Hedrick, J. K. [2007] Optimal Path Planning with a Kinematic Airplane Model. *Journal of Guidance, Control, and Dynamics* **30**(2):629 – 633.

[99] Techy, L., Woolsey, C. A. and Morgansen, K. A. [2010] Minimum-Time Planar Path Planning for Flight Vehicles in Wind with Turn Rate and Acceleration Bounds. In *IEEE International Conference on Robotics and Automation*, 3240 – 3245. Anchorage, AK.

[100] Cartwright, J. H. E., Magnasco, M. O., Piro, O. and Tuval, I. [2002] Bailout embeddings and neutrally buoyant particles in three-dimensional flows. *Physical Review Letters* **89**:264501.

[101] Ross, S. D. [2006] Optimal flapping strokes for self-propulsion in a perfect fluid. In *Proceedings of 2006 American Control Conference*, 4118–4122.

[102] Chang, D. E. and Marsden, J. E. [2003] Gyroscopic forces and collision avoidance with convex obstacles. In *New Trends in Nonlinear Dynamics and Control, and their Applications* (edited by W. Kang, M. Xiao, and C. Borges), vol. 295 of *Lecture Notes in Control and Information Sciences*, 145–160. Springer, Berlin-Heidelberg-New York.

[103] Zhang, F., Justh, E. and Krishnaprasad, P. S. [2004] Boundary following using gyroscopic control. In *Proc. of 43rd IEEE Conf. on Decisions and Control*, 5204–5209.